PREx/CREx Results

P. A. Souder

Syracuse University

U.S. DEPARTMENT OF ENERGY | Office of Science

Jefferson Lab

Shapes of Nuclei

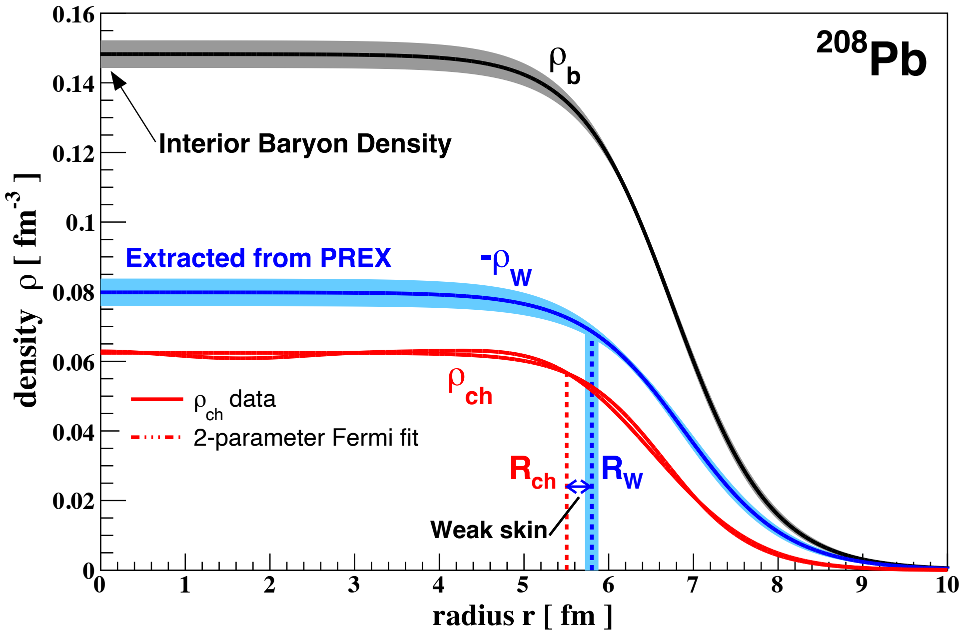

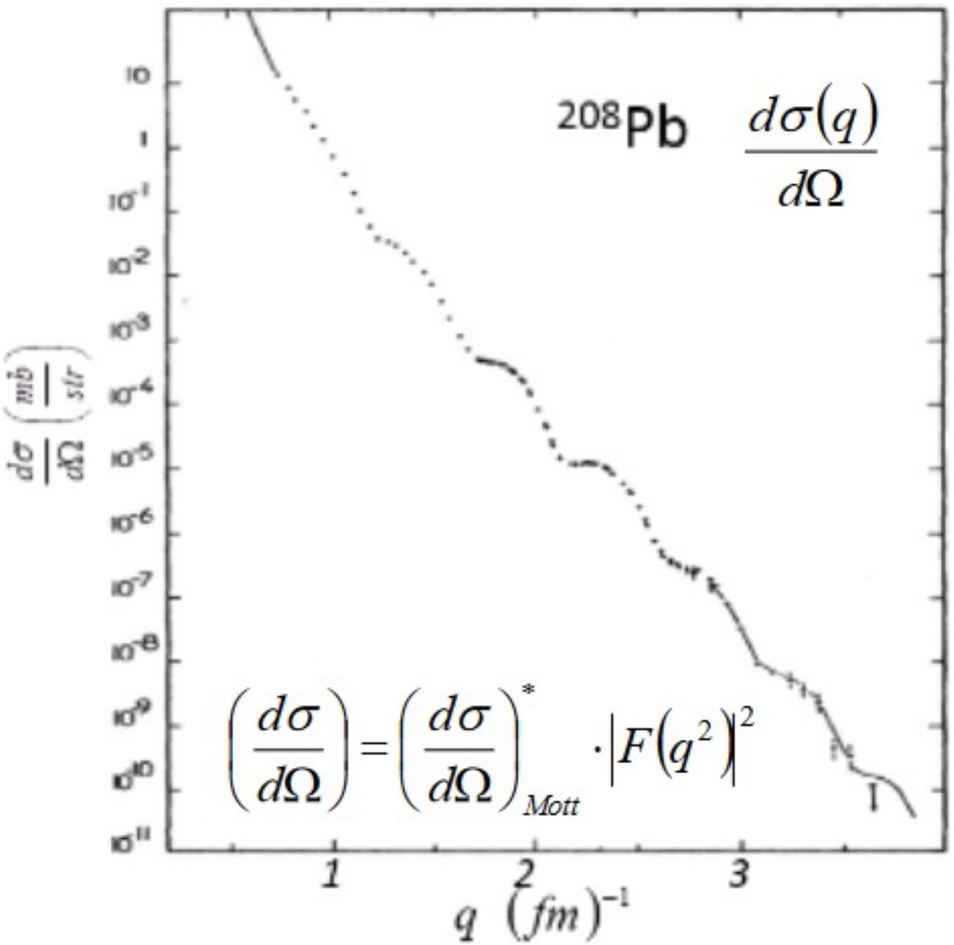

- The excess neutrons in ^{208}Pb are thought to form a skin on the outside of the nucleus
- Similar to how the Fourier transform of the electromagnetic form factor gives charge density so too measuring the weak form factor can give the weak distribution

Parity Violation in Electron Scattering (PVES)

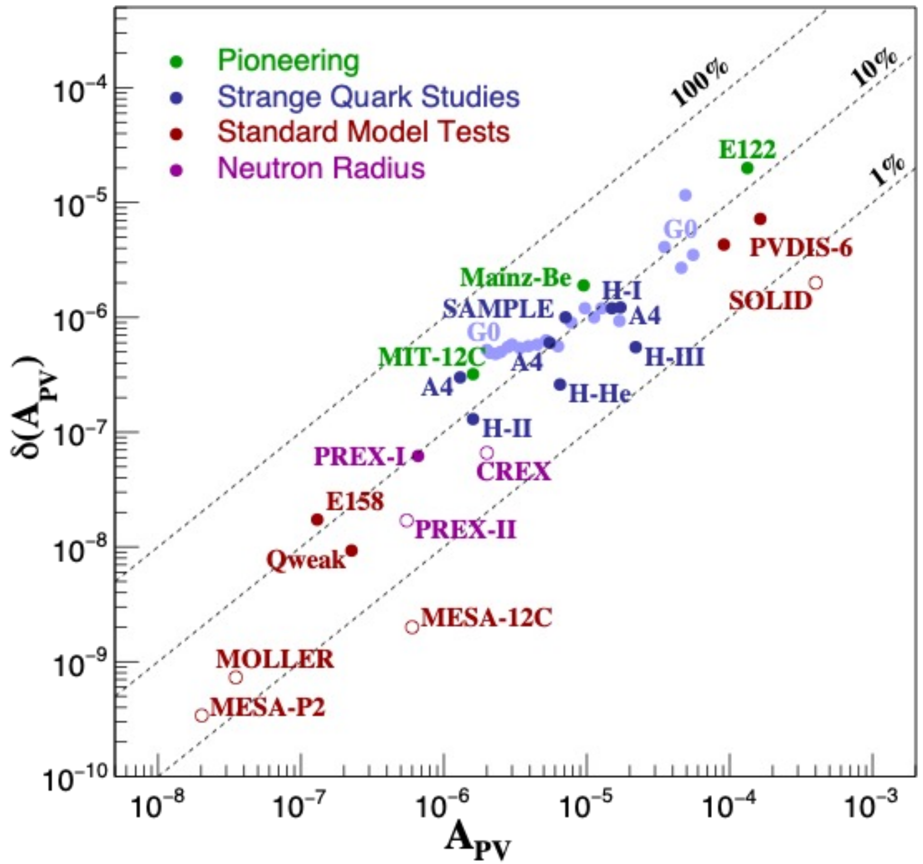

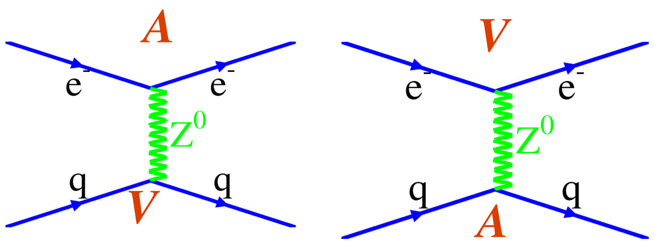

$C_{1i} \equiv 2 g_A^e g_V^i$ $C_{2i} \equiv 2 g_V^e g_A^i$

$$Q_W(Z,N) = -2[C_{1u}(2Z+N) + C_{1d}(Z+2N)]$$

$Q_W(Z,N) = 0.006\ Z + 1.68\ N$

Weak Form Factors and PVES

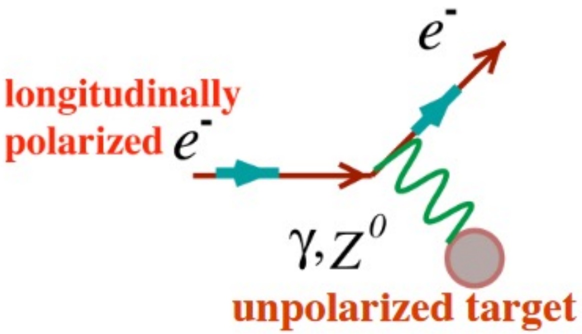

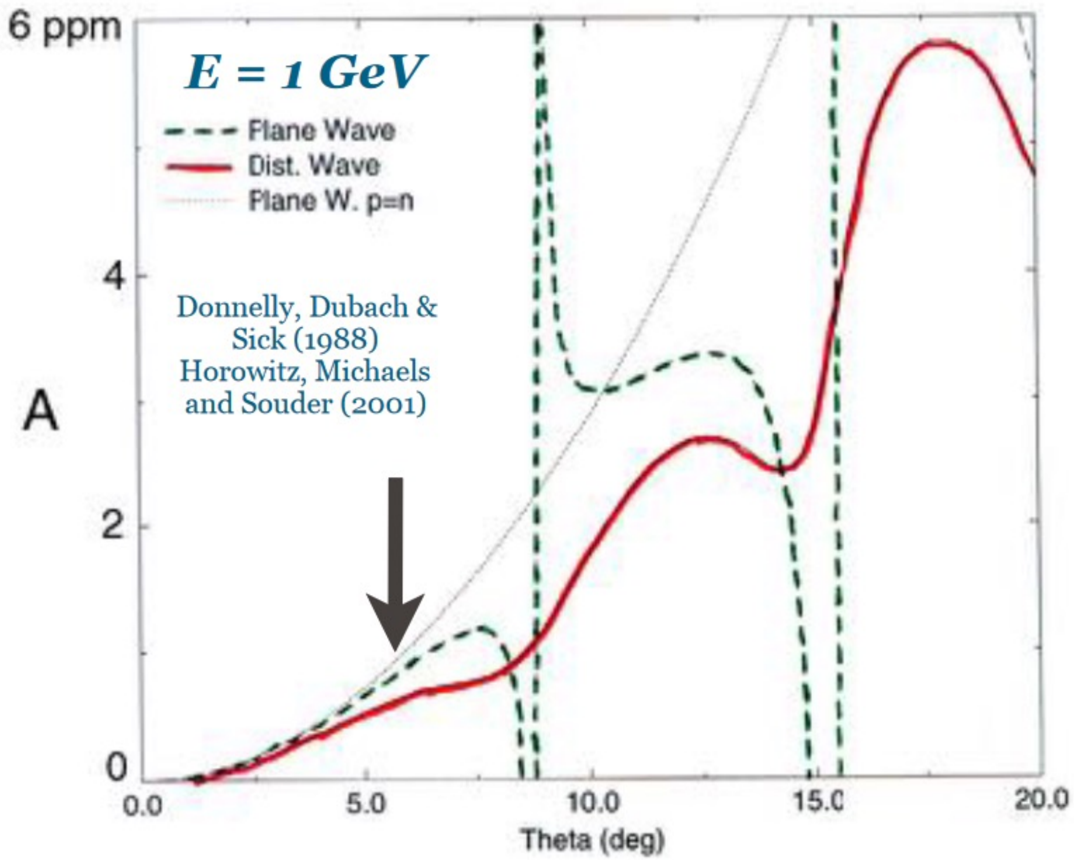

Born approximation: $$A_{PV} \approx \frac{G_F Q^2}{4\pi\alpha\sqrt{2}} \frac{Q_W F_W(Q^2)}{Z F_{ch}(Q^2)}$$

- The numerator is dominated by the gamma-Z interaction which picks up (almost exclusively) the weak charge of the neutron
- The denominator contains the parity conserving electro-magnetic interaction which is several orders of magnitude stronger than the electro-weak interference term
  - This leads to very small asymmetries that are on the level of parts-per-million

First Polarized Electrons, PVES; 1970's

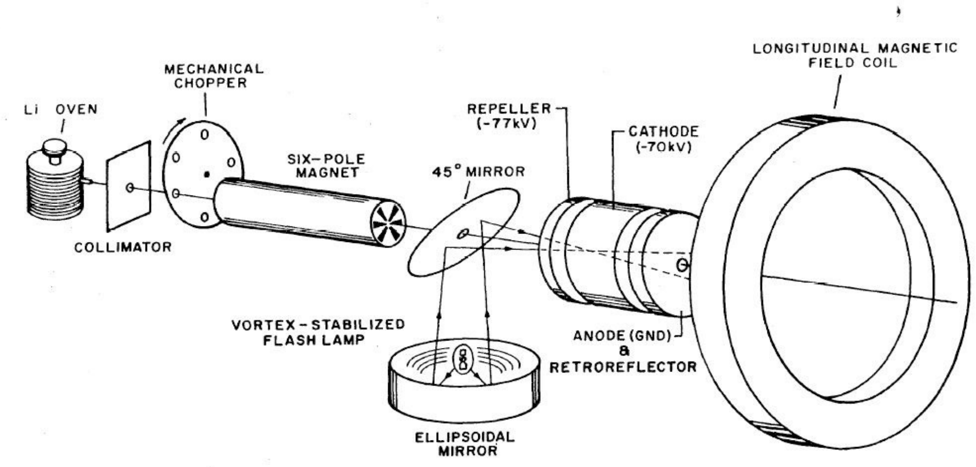

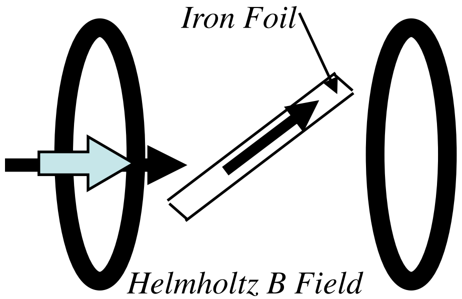

$$\frac{(\sigma_{\uparrow\downarrow} - \sigma_{\downarrow\downarrow})}{(\sigma_{\uparrow\downarrow} + \sigma_{\downarrow\downarrow})} = -\frac{\sin^2\theta(7+\cos^2\theta)}{(3+\cos^2\theta)^2}$$

parity-conserving
purely QED effect

POLARIZED ELECTRON-ELECTRON SCATTERING AT GeV ENERGIES*

P.S. Cooper, M.J. Alguard, R.D. Ehrlich, V.W. Hughes, H. Kobayakawa,† J.S. Ladish,‡ M.S. Lubell, N. Sasao, K.P. Schüler,‡ and P.A. Souder

J.W. Gibbs Laboratory, Yale University, New Haven, CT. 06520

G. Baum and W. Raith

University of Bielefeld, Bielefeld, West Germany

K. Kondo‖

University of Tokyo, Tokyo, Japan

D.H. Coward, R.H. Miller, C.Y. Prescott, D.J. Sherden, and C.K. Sinclair

Stanford Linear Accelerator Center, Stanford, CA. 94305

ABSTRACT

The longitudinal polarization of the new Yale-SLAC polarized electron beam has been determined at laboratory energies between 6.47 and 19.40 GeV. Spin-dependent elastic electron-electron scattering (Møller scattering) has been found to be a practical technique for polarization measurements at high energies. The

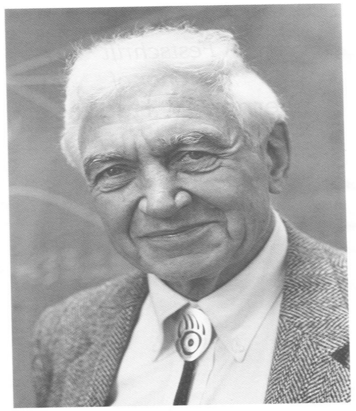

Vernon W. Hughes

Accelerator/Experimental Overview

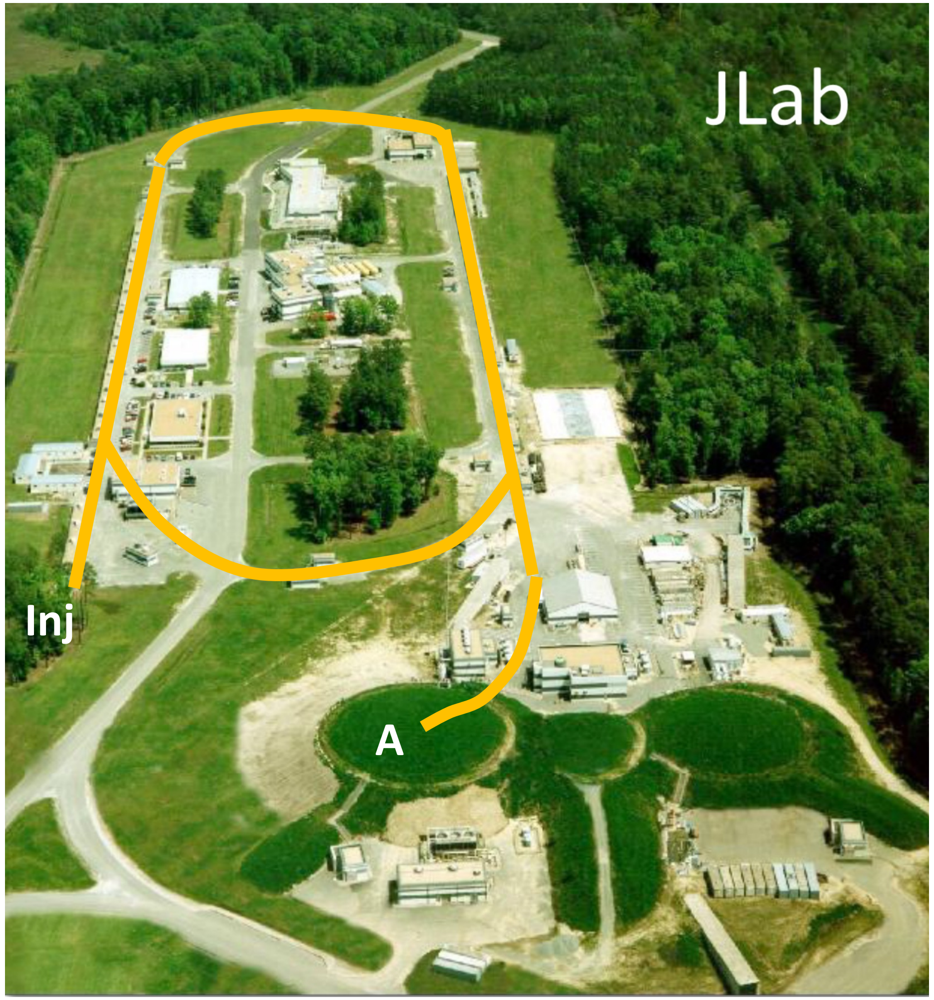

Injector

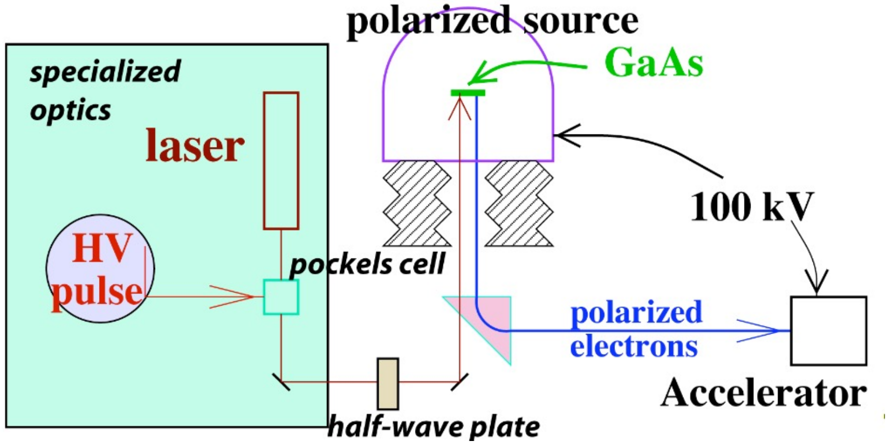

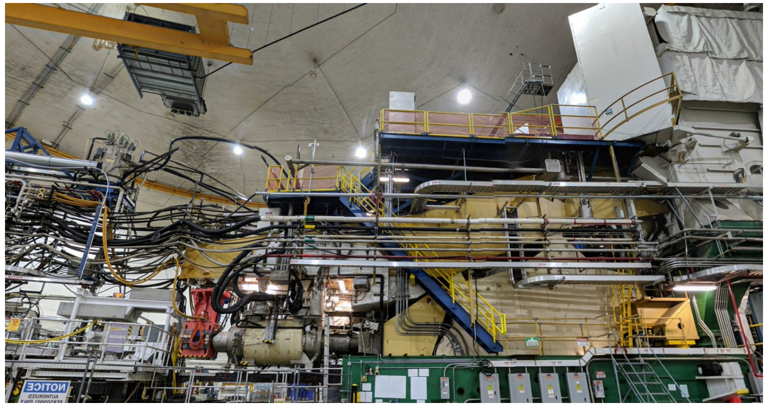

Hall A

- CEBAF is the ONLY operating facility in the world where such an experiment could be attempted

Helicity Reversals

1. Laser Helicity (KHz)
2. Half Wave plate (Hr)
3. Wien flip (slow)

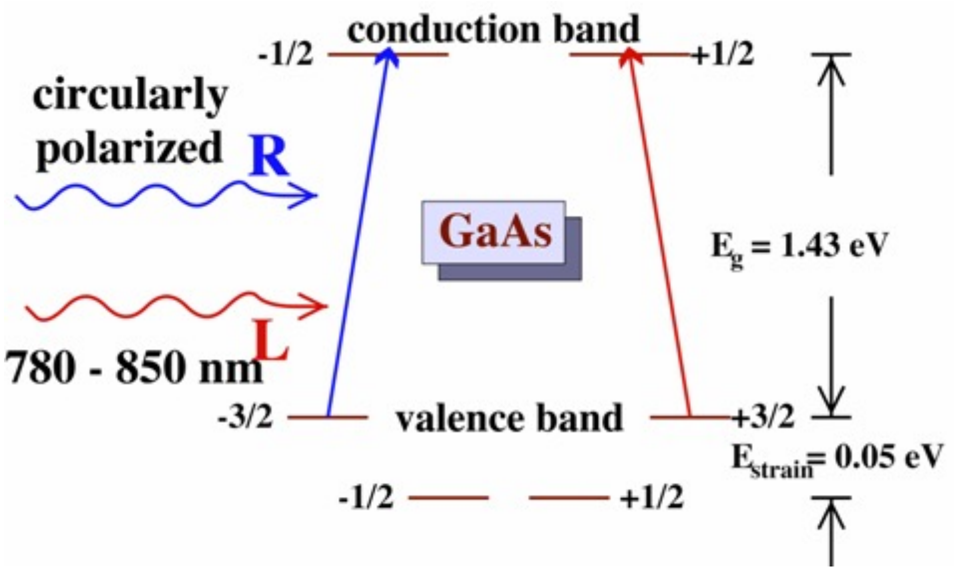

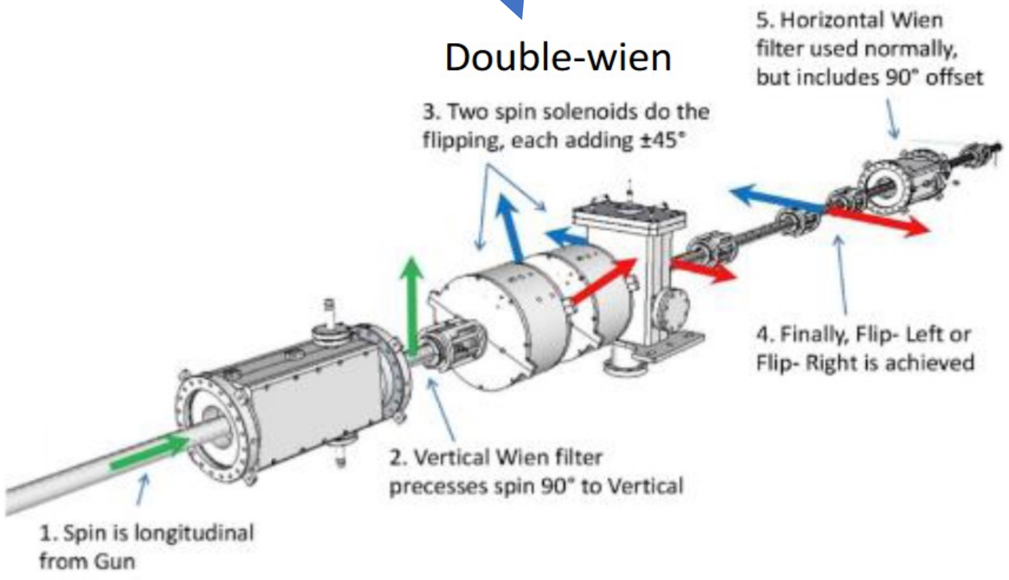

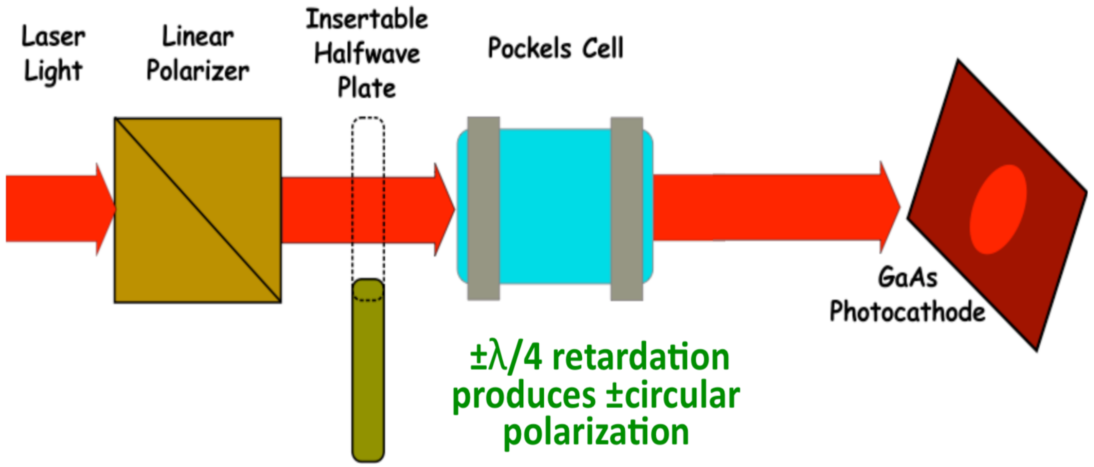

^{208}Pb Targets

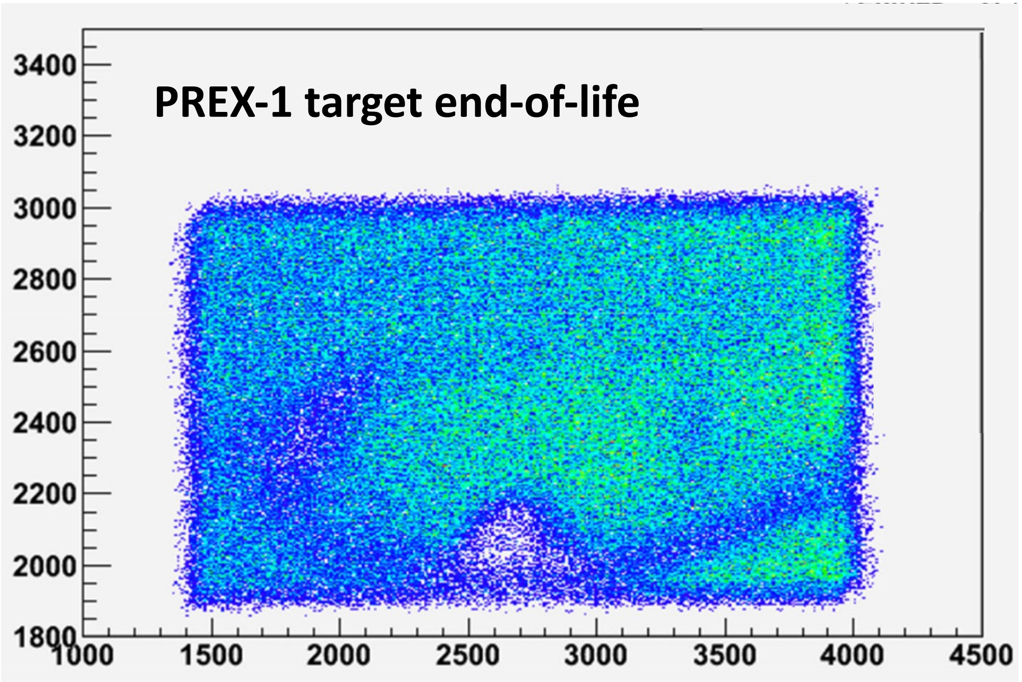

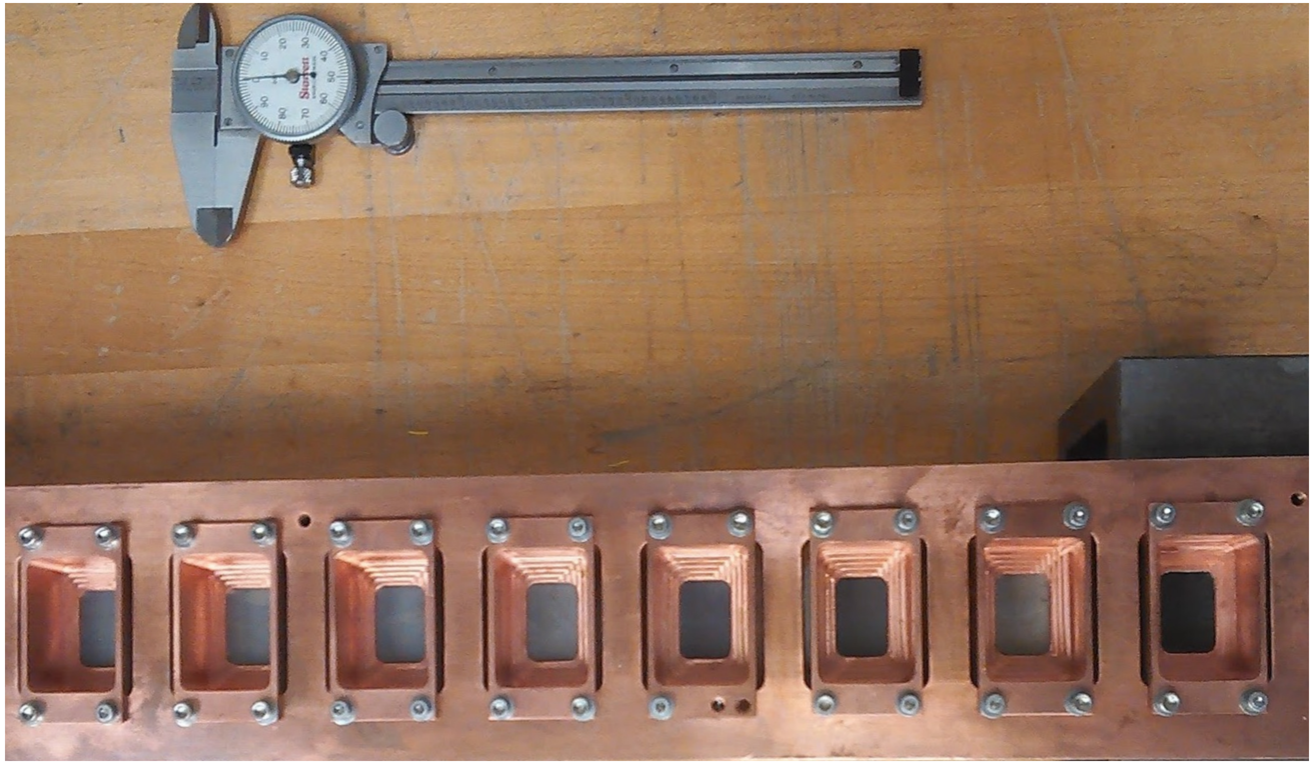

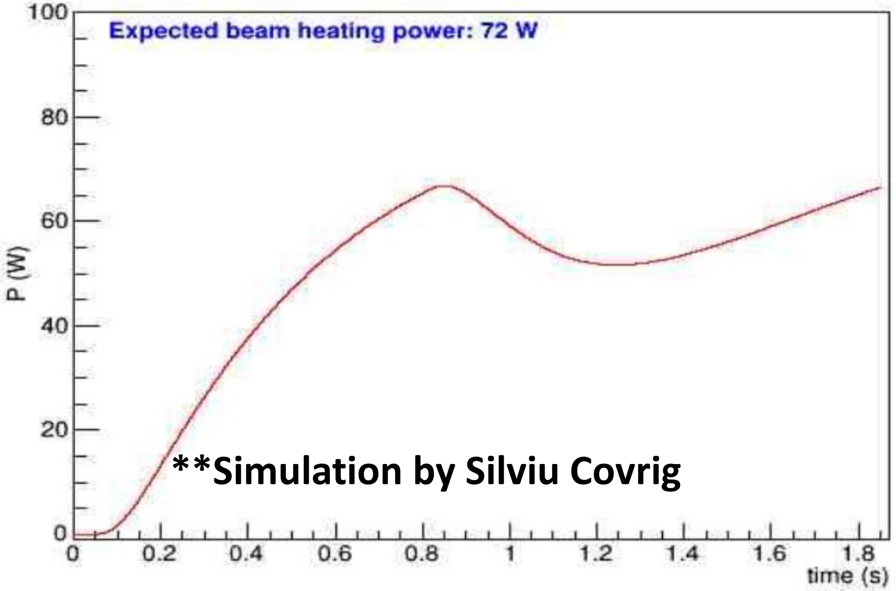

- For PREX we prepared a complement of 10 isotopically pure targets in the expectation that we would use approximately 6

Absolute Angle Calibration - Watercell

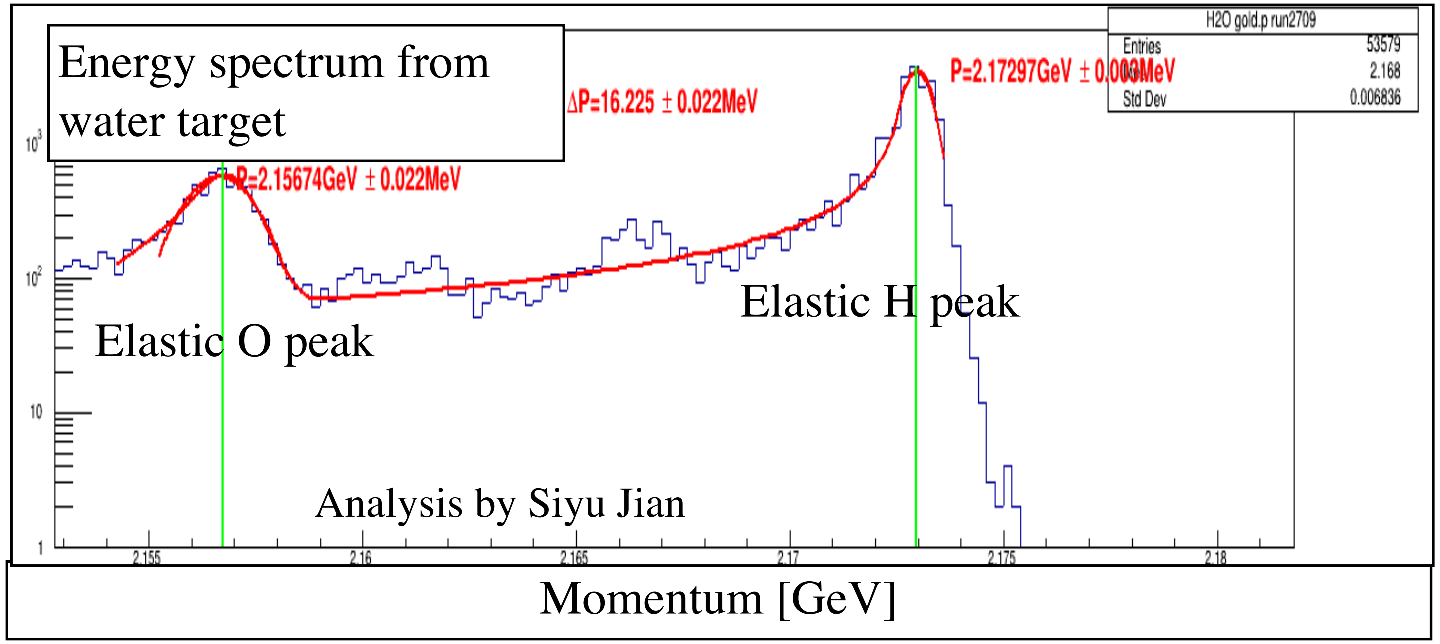

- Critical to measure the absolute scattering angle to high precision
- Nuclear recoil method
- ^{1}H and ^{16}O in one target (same E-loss) provides straightforward measurement of angle, insensitive to other calibrations

$$A_{PV} \approx \frac{G_F Q^2}{4\pi\alpha\sqrt{2}} \frac{Q_W F_W(Q^2)}{Z F_{ch}(Q^2)}$$

recoil momentum difference $\longrightarrow$ scattering angle

$$\Delta E' = E'_O - E'_H = E\left(\frac{1}{1+\frac{2E\sin^2(\frac{\theta}{2})}{M_O}} - \frac{1}{1+\frac{2E\sin^2(\frac{\theta}{2})}{M_H}}\right)$$

Determined central angle with pointing with precision of $\delta\theta = 0.02^0$ (0.45%)

Spectrometer Isolates Elastic events

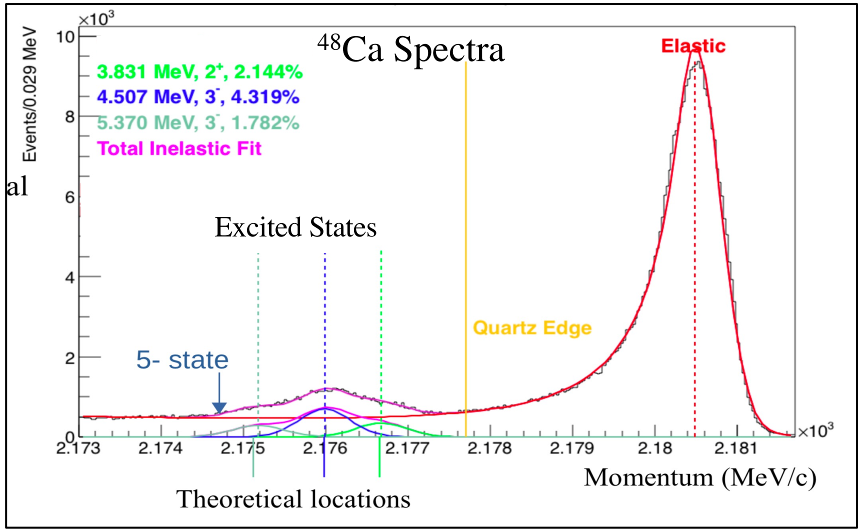

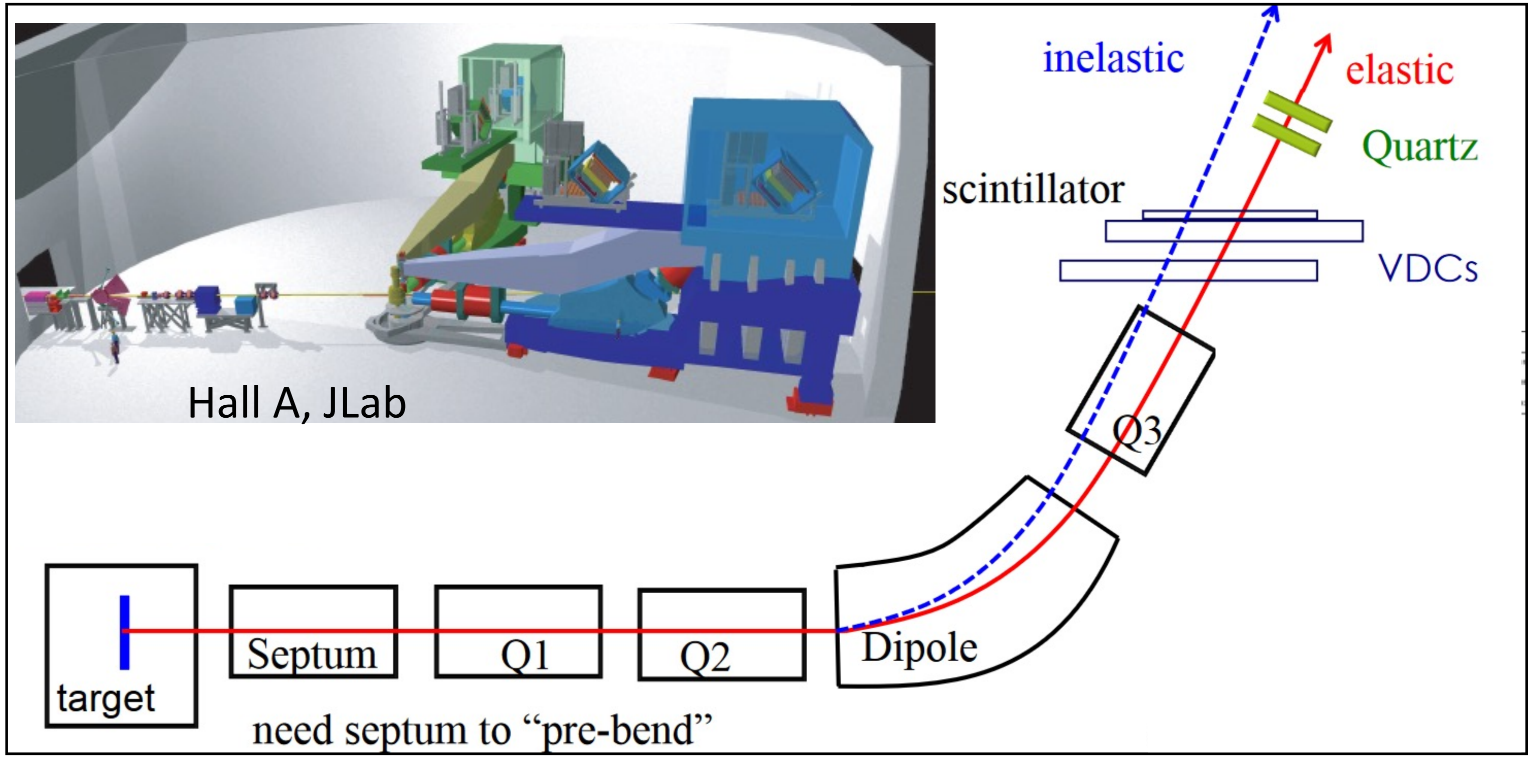

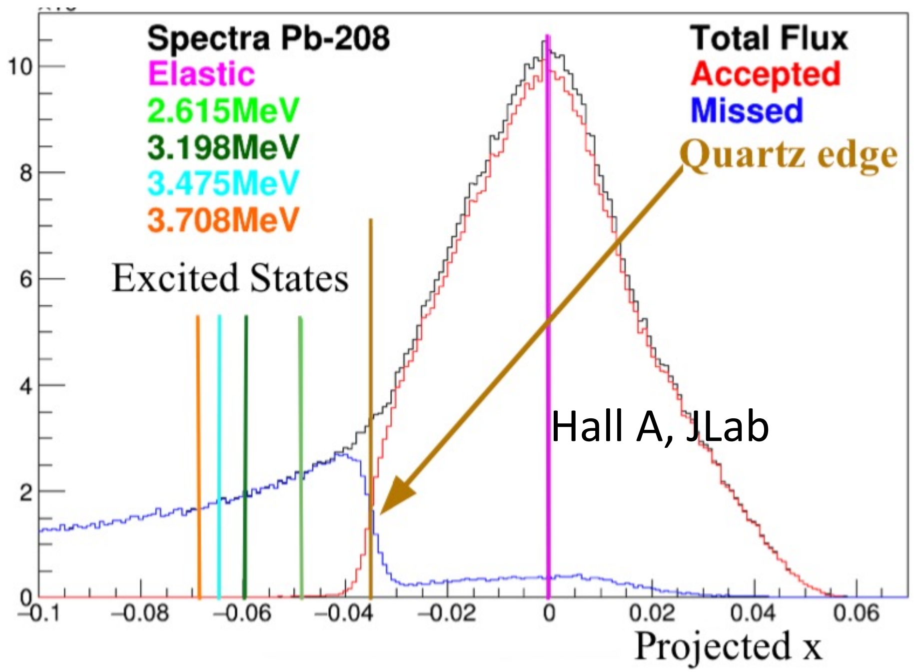

Integrating electronics

- The challenge: all electrons need to count the same
  - While a thicker “quartz” (fused silica) would give you larger number of photo-electrons it also increase the likelihood of showers which introduces noise to width
- The signal rate was approximately 2.2 Ghz in a 3x3 cm^2 area at the end of the detector

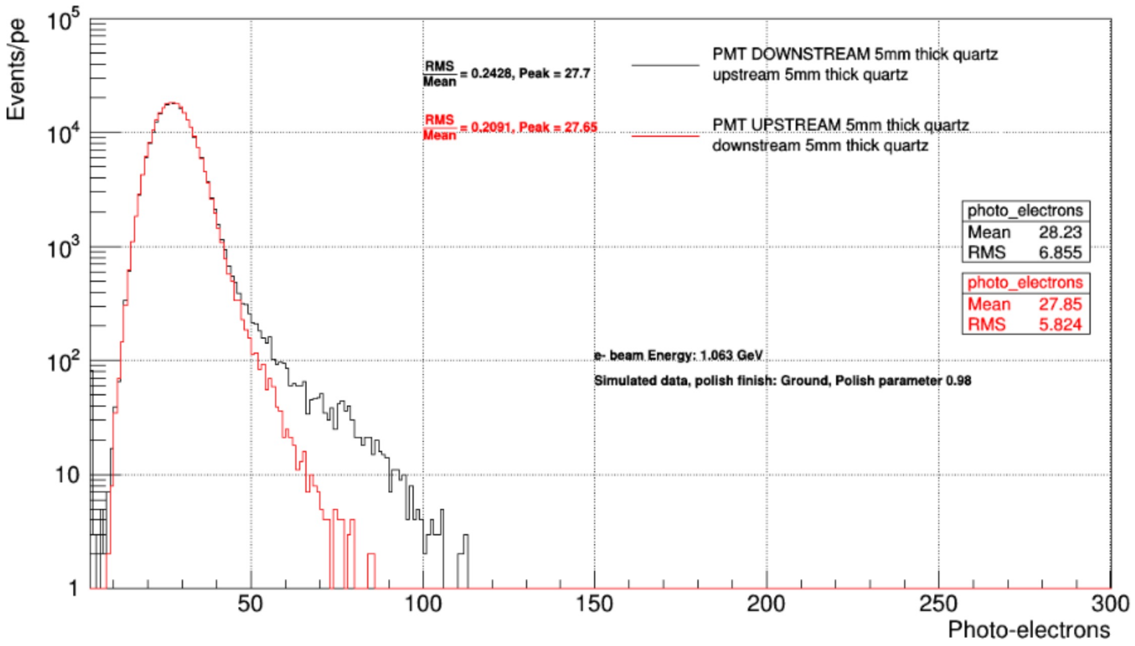

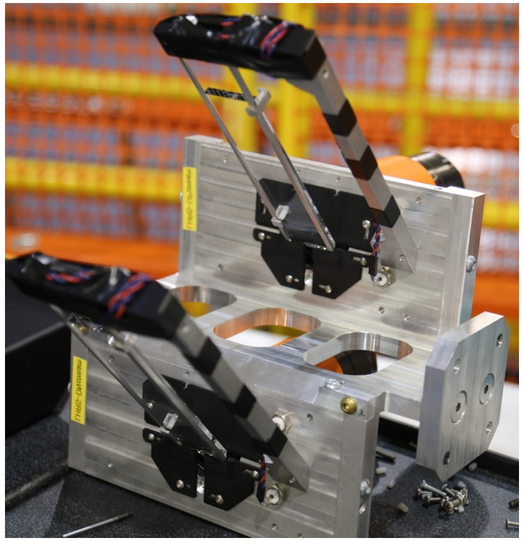

Repeat Many Times (PREx Data)

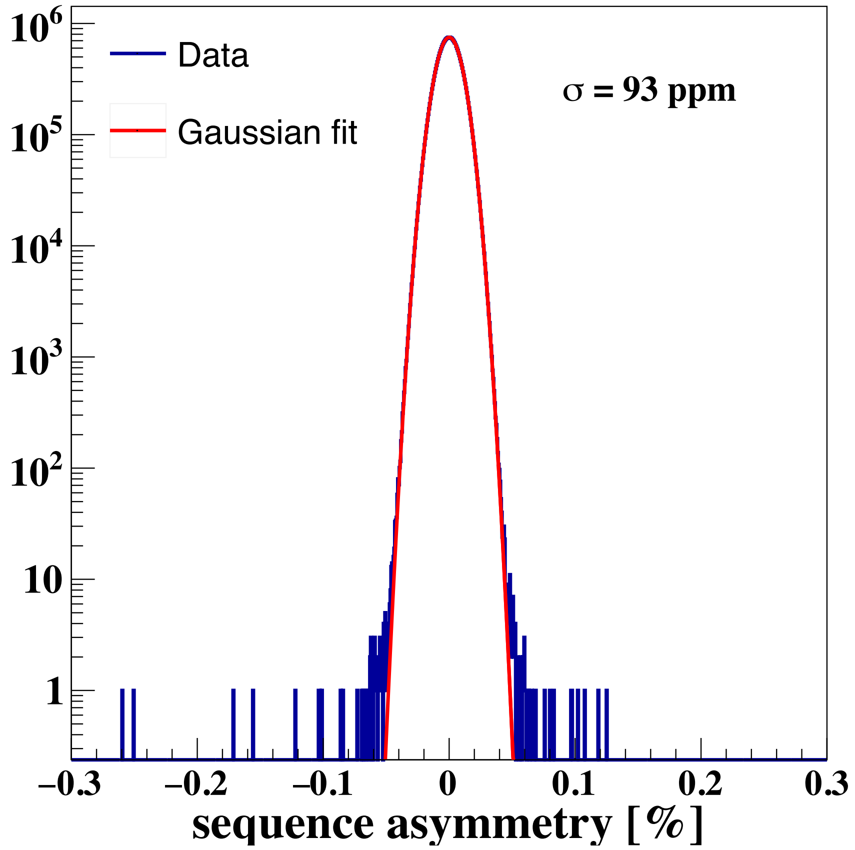

FIG. 1. Distribution of 30 million asymmetries measured over 1/30 s sequences formed with 240 Hz helicity flips. Only data taken with a beam current near to 70 μA is included.

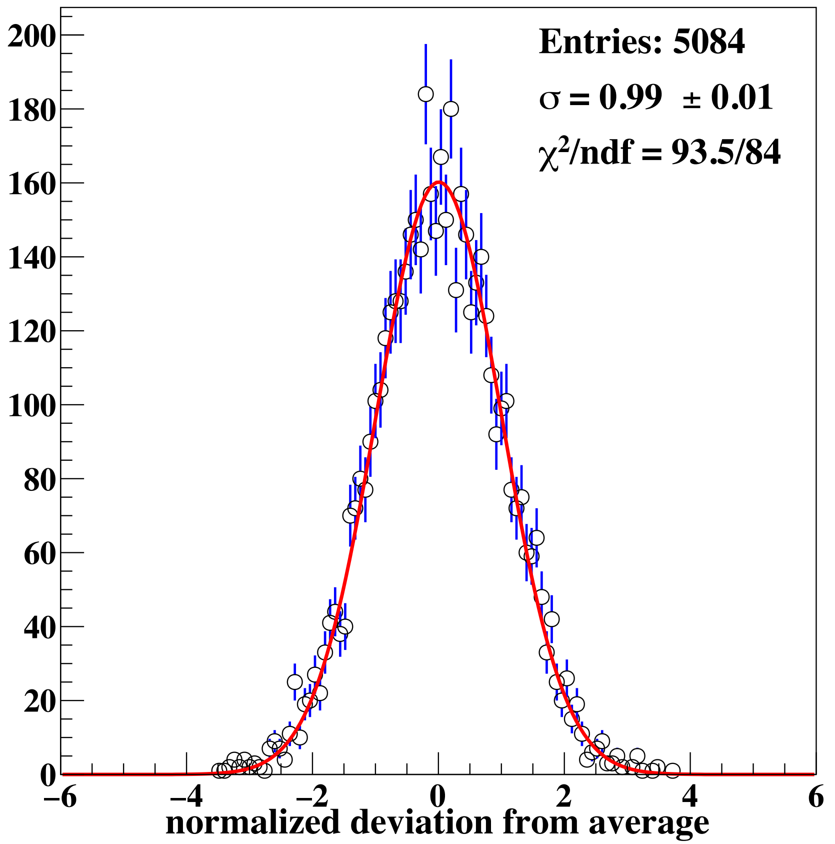

FIG. 2. Distribution of normalized deviations from the average (blue) for ≈5-minute asymmetry datasets after beam corrections, compared to a Gaussian fit(red).

Beam Modulation

- To span the 5 dimension phase space of beam motion at the target (position, angle, energy) we made use of a set of 6 coils and an energy vernier
  - The extra set of air-core dipoles (coils) can be used as a cross check to confirm our procedure doesn't introduce unwanted noise
  - This modulation is automated and was performed throughout the data taking period

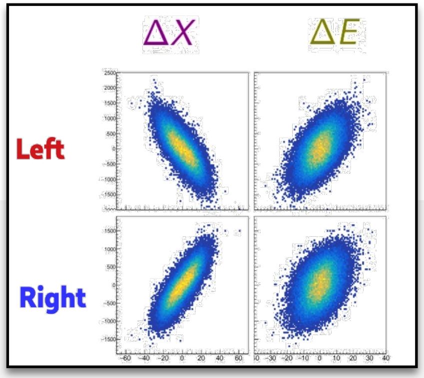

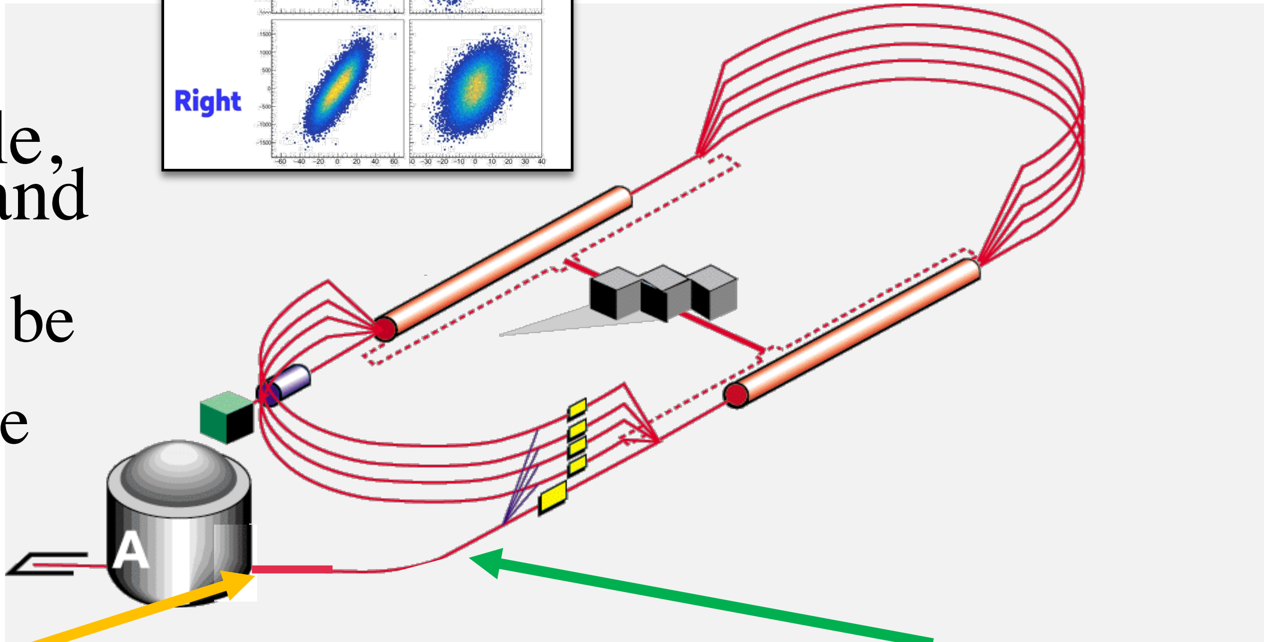

Beam monitors determine trajectory and parameters onto target

Beam modulation system spans the phase space of beam motion

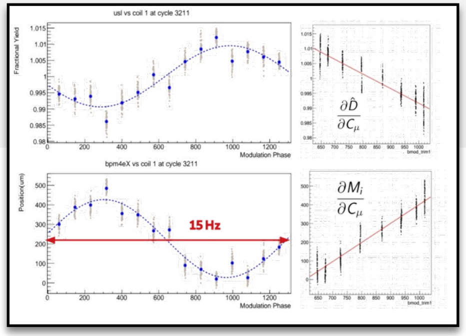

Beam Corrections

- Steep form-factor and very forward angle: very sensitive to beam corrections. Beam jitter noise several times greater than counting statistics
- Corrections narrow width to improve statistics
- Corrections remove systematic errors
- Potential for systematic error if average beam asymmetries are not well corrected

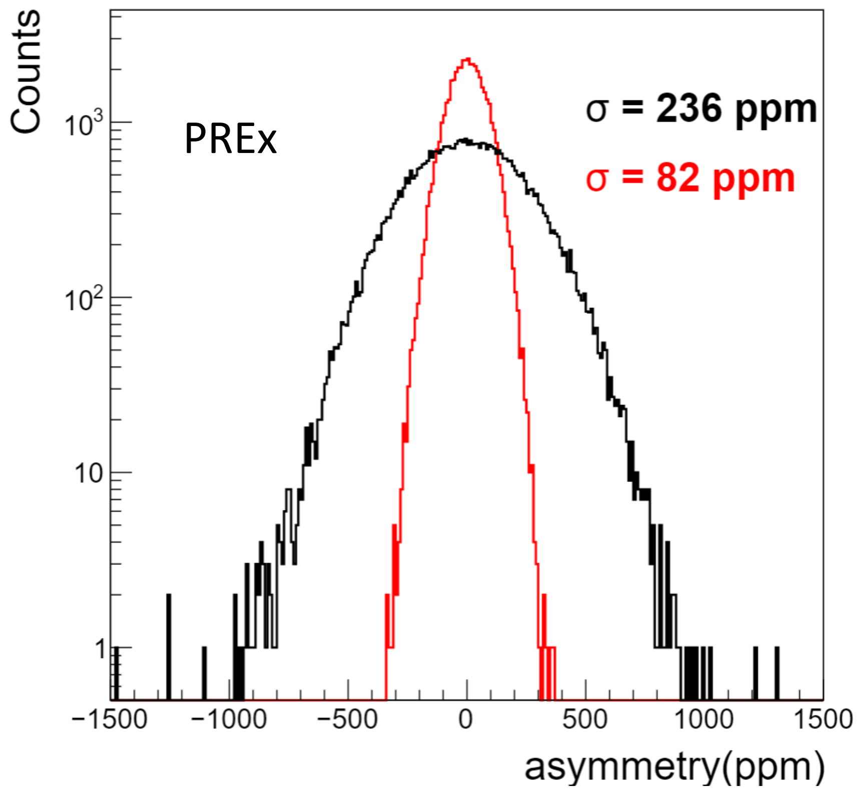

$$A = A_{raw} - A_Q - \sum_i \alpha_i \Delta x_i - \alpha_E A_E$$

- Multiple techniques used to calibrate the correction factors (α_i)
- Lots of fancy math used: eg. Lagrangian multipliers…

Cancel Systematics with Slow Flips

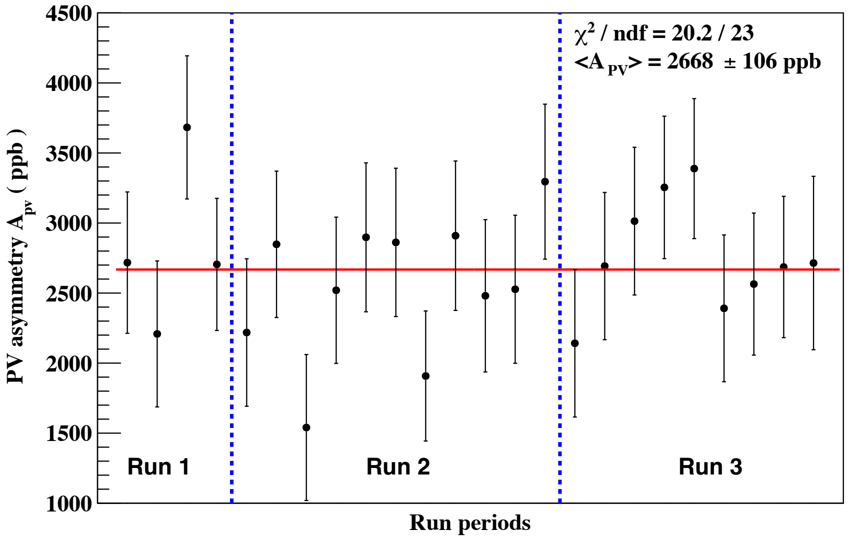

FIG. 1. Measurements of A_{PV} with statistical uncertainty; each ≈40 hour period includes two states with complementary HWP settings. The three run periods demarcate injector spin orientation reversals.

Polarimetry

Compton Polarimetry

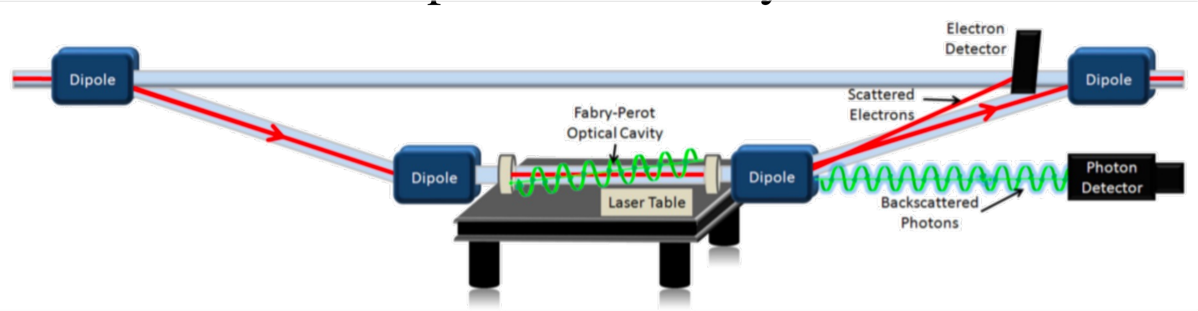

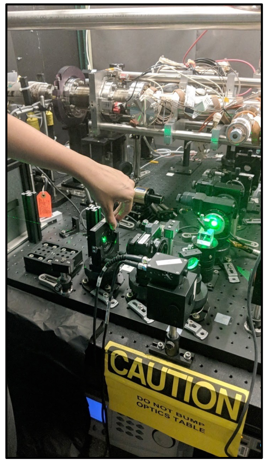

- Continuous, non-invasive measurement
- Utilized integrating technique with photon detector
- Polarimeter runs taken continuously alongside main detector data

Moller Polarimetry

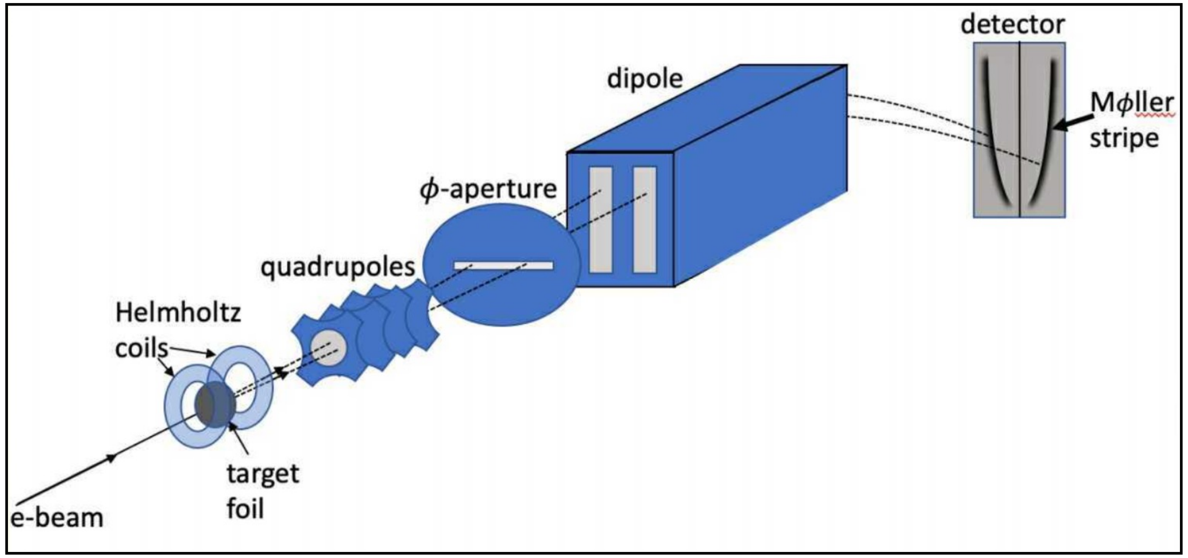

- Low-current, invasive measurement
- 3-4T field provides saturated magnetization perpendicular to the foil
- Polarimeter runs were taken approximately every few days

Compton + Moller polarimeter results, over the run

1 Spring
Right (In/Out)

2 Spring
Left (In/Out)

3 Summer
Right (In/Out)

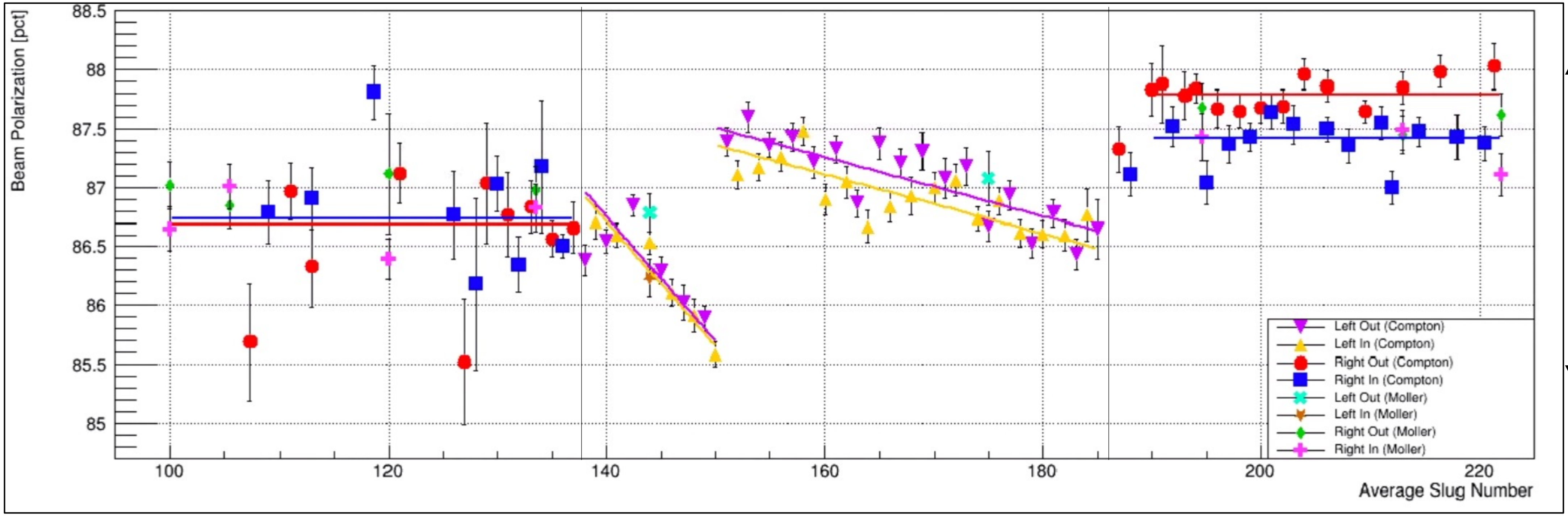

Spans ~ +-1.3% relative error

Acknowledgments: A.J. Zec, J. C. Cornejo, M. Dalton, C. Gal, D. Gaskell, C. Palatchi, K. Paschke, A. Premithilake, B. Quinn

Average Compton polarization:
87.10 ± (0.52% dP/P)

CREX Polarimetry Result:
P_e=87.09 +/- (0.44% dP/P)

Average Moller polarization:
87.06 ± (0.85% dP/P)

PREx Results and Systematics

Blinded A_{PV}:
(549.4 ± 16.1)ppb

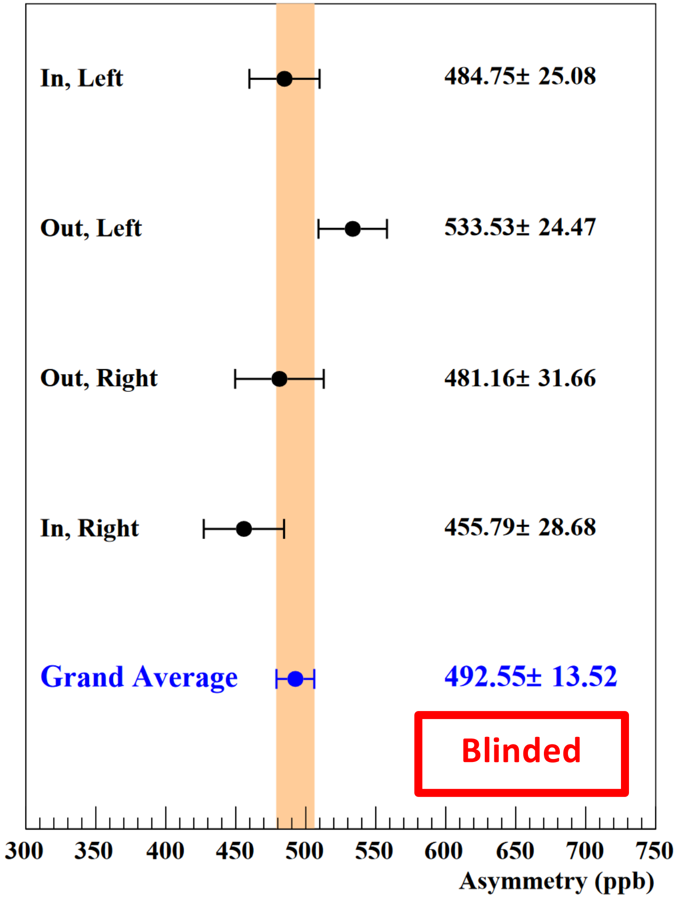

TABLE I. Corrections and systematic uncertainties to extract A_{PV}^{meas} listed on the bottom row with its statistical uncertainty.

Correction	Absolute [ppb]	Relative [%]
Beam asymmetry	-60.4 ± 3.0	11.0 ± 0.5
Charge correction	20.7 ± 0.2	3.8 ± 0.0
Beam polarization	56.8 ± 5.2	10.3 ± 1.0
Target diamond foils	0.7 ± 1.4	0.1 ± 0.3
Spectrometer rescattering	0.0 ± 0.1	0.0 ± 0.0
Inelastic contributions	0.0 ± 0.1	0.0 ± 0.0
Transverse asymmetry	0.0 ± 0.3	0.0 ± 0.1
Detector nonlinearity	0.0 ± 2.7	0.0 ± 0.5
Angle determination	0.0 ± 3.5	0.0 ± 0.6
Acceptance function	0.0 ± 2.9	0.0 ± 0.5
Total correction	17.7 ± 8.2	3.2 ± 1.5
A_{PV}^{meas} and statistical error	550 ± 16	100.0 ± 2.9

$$A_{PV} = R_{acceptNorm} \frac{A_{corr}/P_e - \sum_i A_i f_i}{1 - \sum_i f_i}$$

$$A_{corr} = A_{raw} + A_{beam} + A_{nonLin} - A_{blind}$$

CREx Results and Systematics

Blinded Corrected Asymmetry A_{corr}:
2080.3 ± 84 ppb

$$A_{corr} = A_{det} - A_{beam} - A_{trans} - A_{nonlin} - A_{blind}$$

$$A_{phys} = R_{radcorr}\, R_{accept}\, R_{Q^2} \frac{A_{corr} - P_L \sum_i f_i A_i}{P_L(1 - \sum_i f_i)}$$

Blinded A_{PV}:
2334.8 ± 106 (stat) ± 40 (sys)ppb
[± 112 ppb(tot)]

Correction	Absolute [ppb]	Relative [%]
Beam polarization	382 ± 13	14.3 ± 0.5
Beam trajectory & energy	68 ± 7	2.5 ± 0.3
Beam charge asymmetry	112 ± 1	4.2 ± 0.0
Isotopic purity	19 ± 3	0.7 ± 0.1
3.831 MeV (2^+) inelastic	-35 ± 19	-1.3 ± 0.7
4.507 MeV (3^-) inelastic	0 ± 10	0 ± 0.4
5.370 MeV (3^-) inelastic	-2 ± 4	-0.1 ± 0.1
Transverse asymmetry	0 ± 13	0 ± 0.5
Detector non-linearity	0 ± 7	0 ± 0.3
Acceptance	0 ± 24	0 ± 0.9
Radiative corrections (Q_W)	0 ± 10	0 ± 0.4
Total systematic uncertainty	40 ppb	1.5%
Statistical uncertainty	106 ppb	4.0%

Unblinding the Data

Blinded A_{PV}:
(549.4 ± 16.1)ppb

Blinded A_{PV}:
2334.8 ± 112.4ppb (4.8%)

Unblinded A_{PV}:
(550.0 ± 16.1)ppb

Unblinded A_{PV}:
2658.6 ± 113.2ppb (4.3%)

"Blinding box": an additive term on every octet asymmetry, randomly selected (flat) at the start of the run, from ± 160 (900) ppb for PREx (CREx)

Extracting R_W from A_{PV}

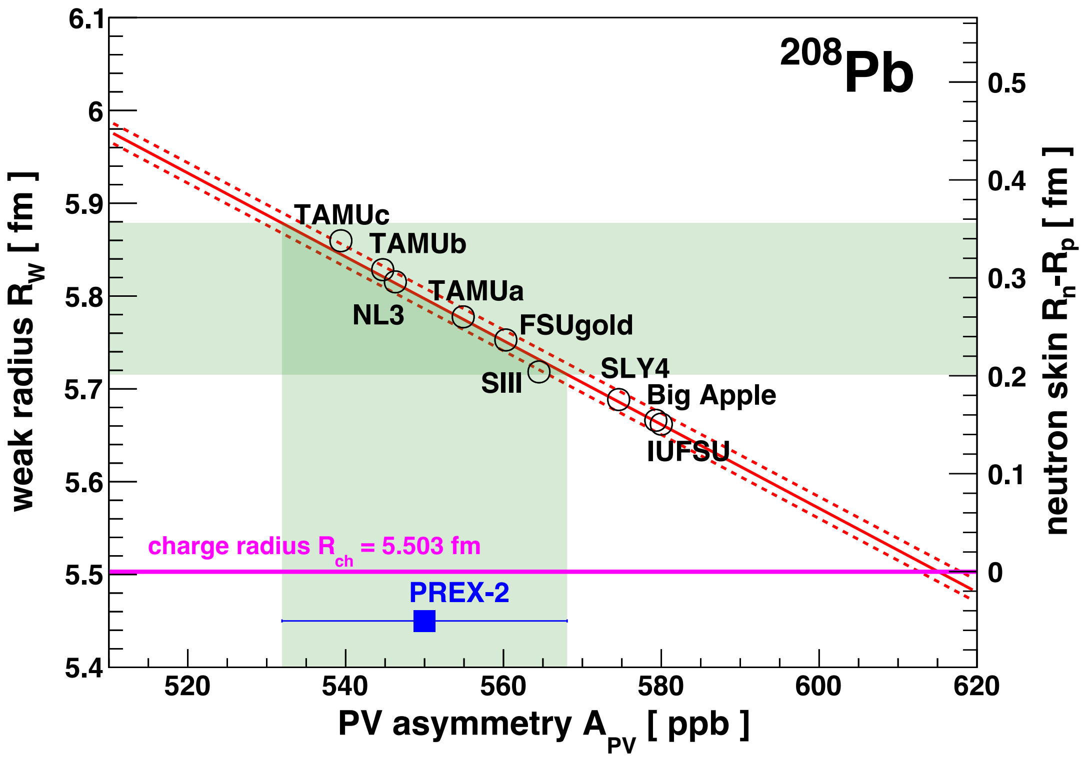

FIG. 3. Extraction of the weak radius (left vertical axis) or neutron skin (right vertical axis) for the ^{208}Pb nucleus. R_{ch} [46] is shown for comparison.

Extracting R_W and R_n from CREx Data

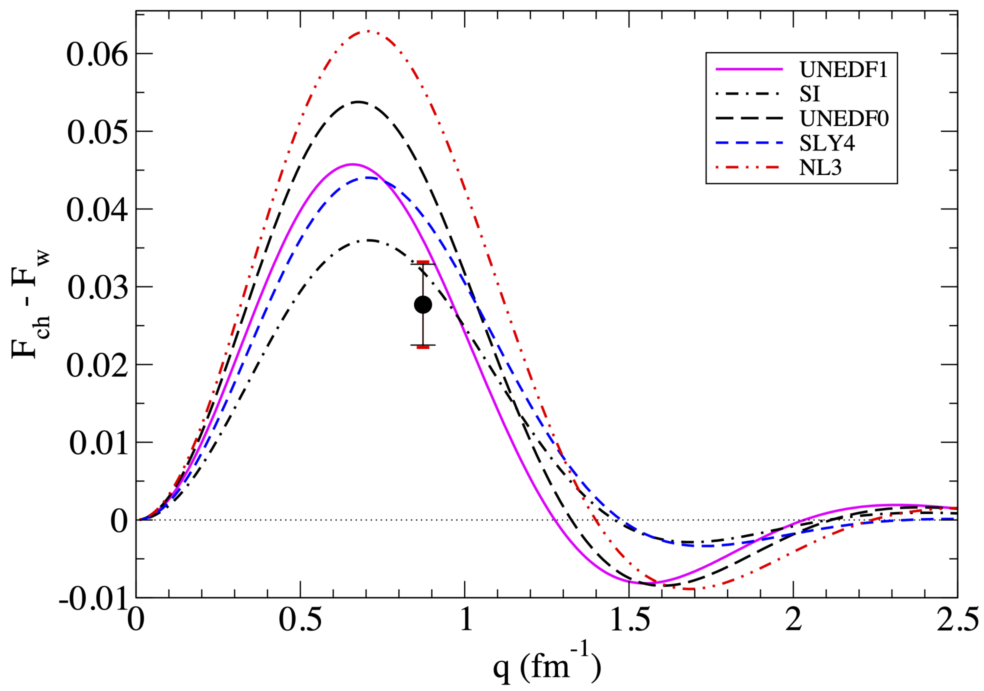

FIG. 3. The difference between the charge and weak form factors for ^{48}Ca as a function of momentum transfer $q = \sqrt{Q^2}$. The curves show results for non-relativistic (SI, SLY4, UNEDF0, UNEDF1) and relativistic (NL3) density functional models. The CREX measurement is indicated by a circle with the inner black error bar showing the contribution from statistics and the total experimental error bar in red.

Extracting R_W and R_n from CREx Data-II

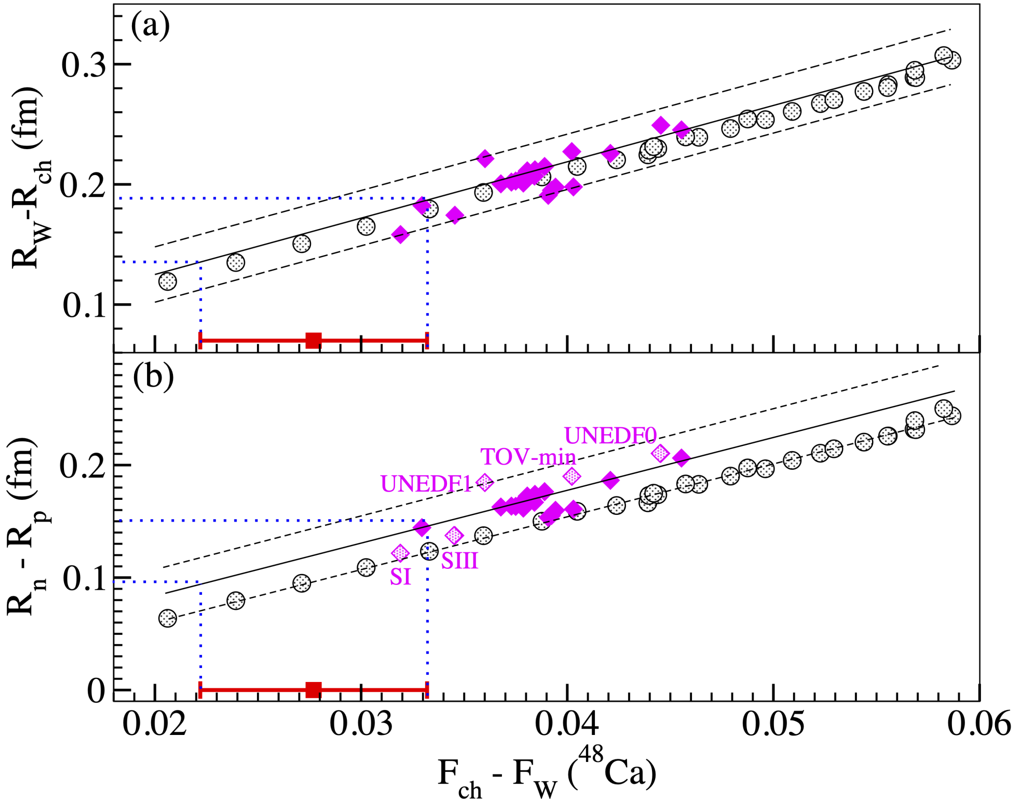

FIG. 4. (a) ^{48}Ca weak minus charge rms radius versus charge minus weak form factor at the CREX momentum transfer. The CREX experimental value and uncertainty is shown (red square). The gray circles (magenta diamonds) show a range of relativistic (non-relativistic) density functionals. (b) ^{48}Ca neutron minus proton rms radius versus charge minus weak form factor.

PREx, CREx, and Models

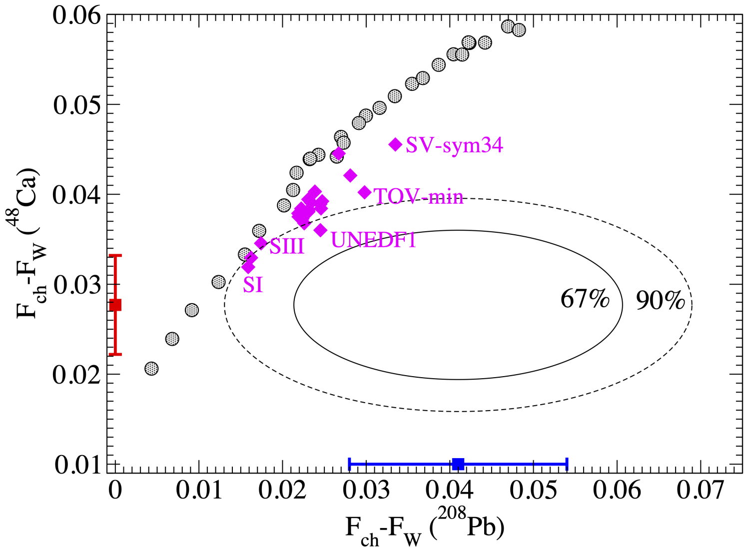

FIG. 2. Difference between the charge and weak form factors of ^{48}Ca (CREX) versus that of ^{208}Pb (PREX-2) at their respective momentum transfers. The blue (red) data point shows the PREX-2 (CREX) measurements. The ellipses are joint PREX-2 and CREX 67% and 90% probability contours. The gray circles (magenta diamonds) are a range of relativistic (non-relativistic) density functionals. For clarity only some of these functionals are labeled. The complete list is in ref. [31].

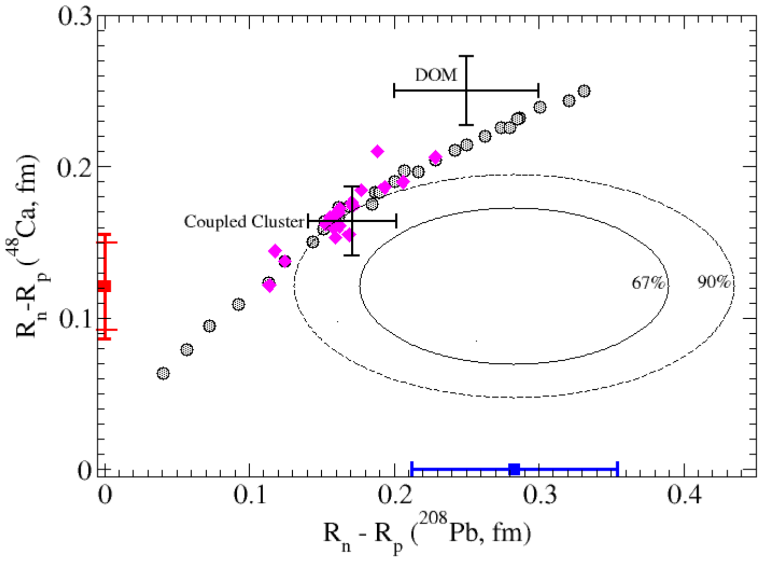

FIG. 5. ^{48}Ca neutron minus proton radius versus that for ^{208}Pb. The PREX-2+PREX-1 experimental result is shown as a blue square, while that for CREX is shown as a red square with the inner error bars indicating the experimental error and the outer error bars including the model error. The gray circles (magenta diamonds) show a variety of relativistic (non-relativistic) density functionals. Coupled cluster [8] and dispersive optical model (DOM) predictions [46] are also shown.

PREx/CREx Collaborators

Students: Devi Adhikari, Devaki Bhatta Pathak, Quinn Campagna, Yufan Chen, Cameron Clarke, Catherine Feldman, Iris Halilovic, Siyu Jian, Eric King, Carrington Metts, Marisa Petrusky, Amali Premathilake, Victoria Owen, Robert Radloff, Sakib Rahman, Ryan Richards, Ezekiel Wertz, Tao Ye, Adam Zec, Weibin Zhang

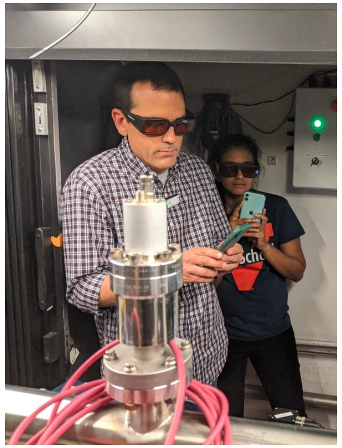

Post-docs and Run Coordinators: Rakitha Beminiwattha, Juan Carlos Cornejo, Mark-Macrae Dalton, Ciprian Gal, Chandan Ghosh, Donald Jones, Tyler Kutz, Hanjie Liu, Juliette Mammei, Dustin McNulty,
Caryn Palatchi, Sanghwa Park, Ye Tian, Jinlong Zhang

Spokespeople: D. McNulty, J. Mammei, P. Souder, S. Covrig Dusa, R. Michaels, K. Paschke, S. Riordan, G. Urciuoli, K. Kumar

Hall A techs, Machine Control and other Jefferson Lab staff have been invaluable to this experiment!

Special thanks to: Charles Horowitz and Jorge Piekarewicz for support and insightful conversations
Especially Chuck and grad student Brendan Reed who spent the last three days helping us interpret our results